Subduction polarity reversal facilitated by plate coupling during arc-continent collision: Evidence from the Western Kunlun orogenic belt, NW China

Zaili Tao[1, 2], Jiyuan Yin[1*], Christopher J. Spencer[3], Min Sun[4], Wenjiao Xiao[5*], Andrew C. Kerr[6], Tao Wang[1], Pengpeng Huangfu[7], Yunchuan Zeng[2], Wen Chen[1]

[1] *SinoProbe Laboratory, MNR Key Laboratory of Isotope Geology, Institute of Geology, Chinese Academy of Geological Sciences, Beijing 100037, China*

[2] *School of Earth Sciences and Resources, China University of Geosciences, Beijing, 100083, China*

[3] *Department of Geological Sciences and Geological Engineering, Queen's university, Kingston, Ontario, Canada, K7L 3N6*

[4] *Department of Earth Sciences, the University of Hong Kong, Pokflam Road, Hong Kong, China*

[5] *Xinjiang Institute of Ecology and Geography, Chinese Academy of Sciences, Urumqi, 830011, China*

[6] *School of Earth and Environmental Sciences, Cardiff University, Cardiff, Wales CF10 3AT, United Kingdom*

[7] *College of Earth and Planetary Sciences, University of Chinese Academy of Sciences, Beijing 100049, China*

*Corresponding author: Jiyuan Yin (yinjiyuan1983@163.com);

Wenjiao Xiao (wj-xiao@mail.iggcas.ac.cn)

ABSTRACT

Subduction polarity reversal usually involves the break-off or tearing of the downgoing plate (DP) along the continent-ocean transition zone, in order to initiate subduction of the overriding plate (OP) with opposite polarity. Here we propose that subduction polarity reversal can also be caused by DP-OP coupling and can account for the early Paleozoic geological relationships in the West Kunlun Orogenic Belt, NW China. Our synthesis of elemental and isotopic data reveals transient (~2 Myr) changes in the sources of the early Paleozoic arc magmatism in the southern Kunlun terrane. The early stage (ca. 530–487 Ma) magmatic rocks display relatively high εNd(t) (+0.3 to +8.7), εHf(t) (−3.6 to +16.0) and intra-oceanic arc-like features. In contrast, the late-stage (485–430 Ma) magmatic rocks have predominantly negative εNd(t) (−4.5 to +0.3), εHf(t) (−8.8 to +0.9) and higher incompatible trace elements (e.g., Th), similar to the sub-continental lithospheric mantle beneath the Tarim Craton. This abrupt temporal-spatial variation of arc magmatism, together with the detrital zircon evidence, indicate that subduction polarity reversal of the Proto-Tethys Ocean occurred in a period of ~10 Ma, consistent with the time interval reflected by ophiolite age. This rapid polarity reversal corresponds with the absence of ultra-high-pressure [(U)HP] metamorphic and post-collisional magmatic rocks, features normally characteristic of slab break-off or tearing. Numerical modeling shows that this polarity reversal was caused by plate coupling during arc-continent collision. This modified the normal succession of arc-continent collision events, preventing slab break-off or tearing induced buoyant rock rebound and asthenosphere upwelling. This model successfully explains early Paleozoic orogenesis in the West Kunlun Orogenic Belt and may be applied elsewhere where post-collisional magmatic and (U)HP rocks are absent.

Introduction

Subduction polarity reversal is a key process in plate tectonics, and is a significant mechanism in initiating new subduction zones (Kusky and Kidd, 1996; Stern & Gerya, 2018; Crameri et al., 2020). In a traditional plate-tectonic framework, subduction polarity reversal is

generally considered to be initiated through the break-off or tearing of the downgoing plate along an arc-oceanic plateau (e.g., Solomon Arc; Mann & Taira, 2004; Greater Antilles Arc; Kerr et al. 2003) or arc-continent (e.g., Taiwan; Teng et al., 2000; North China; Kusky et al., 2016) collision zone. However, recent numerical modeling indicates that rheological coupling/plate welding may also be critical in subduction polarity reversal (Almeida et al., 2022). In this model, the welded between the downgoing plate (DP) and overriding plate (OP) yield a slab-pull strong enough to drag the OP downwards, leading to subduction polarity reversal (Almeida et al., 2022). This tectonic scenario is hard to verify and determinations of timescale are difficult because the geological record in original active margins would be modified by subsequent slab-slab interaction. Thus, the influence of plate welding on orogeny remains unclear, despite its potential significance in subduction polarity reversal.

The Paleozoic Western Kunlun Orogen Belt (WKOB; Figs. 1A–B) is an accretionary orogen that developed a series thrust faults with different directions (Fig. 1C) due to subduction of the Proto-Tethys Ocean. However, the detailed dynamic processes in this accretionary orogen are poorly understood (Xiao et al., 2003; Zhang et al., 2019). In this study, we show that the temporal-spatial distribution and compositional variation of Paleozoic magmatism can be best explained by subduction polarity reversal of the Proto-Tethys Ocean. Coupled with the results of numerical modeling, we propose a new model that highlights the impact on orogeny of OP-DP coupling during subduction polarity reversal. This model explains the enigmatic features of many collisional orogens, e.g., the lack of (U)HP rocks and post-collision magmatism and improves our understanding of subduction polarity reversal during orogenic events.

Geological Overview and Paleozoic magmatism

The WKOB in NW China (Fig. 1A) recorded accretion and collision orogenesis during closure of the Proto-Tethys Ocean (Xiao et al., 2003). In the Paleozoic, oceanic closure resulted in collision between the SW Tarim craton and the Tianshuihai terrane, forming the

78 southern Kunlun terrane, which contains two subparallel of suture zones, island arc, but lacks
79 (U)HP rocks and Precambrian basement (Fig. 1B; Zhang et al., 2019). The ophiolites and
80 associated accretionary complexes in the southern Kunlun terrane comprise two units: (1) in
81 the Oytag-Kudi suture zone, early Cambrian-late Cambrian (ca. 525–494 Ma) Oytag-Kudi
82 supra-subduction zone (SSZ)-type ophiolitic mélanges (Li and Zhang, 2014), and (2) in the
83 Mazar-Kangxiwa-Subashi suture zone, early Ordovician (ca. 487–485 Ma) Qimanyute SSZ-
84 type ophiolitic mélanges (Zhang et al., 2021) and late Ordovician (455–446 Ma) Subashi
85 normal mid-ocean ridge basalt ophiolitic mélanges (Zha et al., 2022). A series of NW- and
86 SE-vergent thrust faults are developed in the northern and southern of the southern Kunlun
87 terrane, respectively (Fig. 1C; Xiao et al., 2003). The lithology and tectonic setting of WKOB
88 are detailed in the Supplemental Material.

89 In this study, we analyzed new samples and compiled a dataset of the early Paleozoic (ca.
90 530–430 Ma) magmatic rocks (SiO_2 = 43–56 wt.%), and detrital zircon ages of the early
91 Paleozoic sedimentary rocks in the WKOB (Table DR1–5 in the GSA Data Repository[1]).
92 Based on the timing, distribution and geochemical makeup, the magmatic rocks of the WKOB
93 can be divided into two groups. Group 1 magmatic rocks (ca. 530–487 Ma) exhibit large
94 variations and mostly depleted whole-rock Sm-Nd and zircon Lu-Hf isotopic compositions
95 (Figs. 2A–B). The rocks from the southern Kunlun terrane have higher εNd(t) (+0.3 to +8.7)
96 and εHf(t) (−3.6 to +16.0) than those from the Tianshuihai terranes (εNd(t) = −12.9 to +8.1;
97 εHf(t) = +1.3 to +7.9). In contrast, Group 2 magmatic rocks (ca. 485–430 Ma) display mostly
98 enriched whole-rock Sm-Nd and zircon Lu-Hf isotopic compositions (Figs. 2A–B). They
99 mainly exhibit negative εNd(t) (−4.5 to +0.3) and εHf(t) (−8.8 to +0.9) values in the southern
100 Kunlun terrane, similar to the mafic rocks in SW Tarim Craton (εNd(t)= −6.7 to −4.0; εHf(t)=
101 −13.8 to +0.1).

102

103 # Discussion

Timing of arc-continent collision between the Southern Kunlun terrane and Tarim Craton

The timing of the closure of the northern Proto-Tethys Ocean remains unclear, mainly because continental-type (U)HP rocks are absent in the WKOB. However, provenance of detrital zircon in WKOB Paleozoic strata indicates that the ca. 494–490 Ma (maximum depositional age) samples in the southern Kunlun terrane were predominantly derived from early Paleozoic magmatic rocks in the southern Kunlun terrane (peaks at 530–490 Ma; Fig. 3A). The very limited number of Precambrian grains (Fig. 3A) excludes detrital input from the Tianshuihai terrane or the SW Tarim craton, indicating that the northern Proto-Tethys Ocean lay between the Tarim Craton and the southern Kunlun terrane in the late Cambrian.

In contrast, the ca. 481–430 Ma sedimentary samples in the southern Kunlun terrane contain zircon peaks of 450–470 Ma, with two subordinate clusters around 780–840 Ma and 1100–1140 Ma (Fig. 3B). These age patterns are similar to those from the SW Tarim Craton (ca. 450–470, 770–850 and 1100–1150 Ma; Fig. 3C) but are distinct from those in the Tianshuihai terrane (ca. 500–550, 600–660 and 750–850 Ma; Fig. 3D). This indicates that the ca. 481–430 Ma sedimentary rocks in the southern Kunlun terrane received components from the SW Tarim Craton and thus marks the timing of collision between the southern Kunlun terrane and SW Tarim Craton.

It is significant that the Group 1 magmatic rocks in the southern Kunlun terrane have geochemical affinities with forearc basalt and intra-oceanic arc rocks (Fig. 2C; Fig. S3F; Stern et al., 2012). Furthermore, the Paleozoic strata contain no material older than nearby active arcs (Fig. 3A), and so the southern Kunlun terrane was likely an intra-oceanic arc during the Cambrian. Based on these lines of evidence, we interpret the change in detrital zircon provenance as a consequence of arc-continent-type collision between the southern Kunlun terrane and Tarim Craton in the early Ordovician (490–481 Ma).

Sub-arc mantle transition: magmatic-rock isotopic and elemental evidence

Hf-Nd isotopes in Paleozoic magmatic rocks from the southern Kunlun terrane change abruptly to more enriched values at 487–485Ma (Figs. 2A–B), indicating that the original depleted mantle beneath the southern Kunlun terrane was replaced by an enriched mantle source in the early Ordovician (see details in the Supplemental Material). Based on the whole-rock Sr-Nd isotopic values of the early Paleozoic mafic rocks, there are two potential sources of such isotopically enriched mantle, the Tianshuihai and Tarim sub-continental lithospheric mantle (SCLM; Fig. S3E; Liu et al., 2019; Wang et al., 2022). However, only mixing between the Tarim SCLM and depleted mantle reproduces the composition of Group 2 magmatic rocks in the southern Kunlun terrane (red arrow in Fig. 2D). As our detrital zircon investigation demonstrates that the SW Tarim and southern Kunlun terrane had collided before ca. 481 Ma, the Tarim SCLM can provide a potential mantle source for the Group 2 magmatic rocks in the southern Kunlun terrane.

Furthermore, source characteristics of early Paleozoic magmatic rocks (530–430 Ma) exhibit a systematic variation in space and time, as shown by Th/Sm, Th/Yb and Nb/Yb ratios (Figs. 2E–F, Figs. S4–S5). These ratios abruptly increase from Group 1 magmatic rocks to Group 2 magmatic rocks at ca. 485 Ma, and the values for the Group 2 magmatic rocks progressively increase to the composition of the SW Tarim SCLM (Fig. 2E). Spatially, these ratios of Group 2 magmatic rocks in the southern Kunlun terrane gradually increase towards the SW Tarim Craton magmatic suites from south to north (Fig. 2F). Meanwhile, the Group 2 magmatic rocks in the southern Kunlun terrane are compositionally transitional between the SW Tarim Craton magmatic suites with a crustal signature and Group 1 magmatic rocks in the southern Kunlun terrane with an intra-oceanic affinity (Fig. 2C). These features suggest that: (1) the abrupt changes in isotopic and geochemical compositions of magmatic rocks in the southern Kunlun terrane at ca. 485 Ma were caused by a sub-arc mantle transition from depleted oceanic mantle to enriched Tarim SCLM; and (2) the magnitude of the Tarim

SCLM's influence varied temporally and spatially, increasing from ca. 485 Ma to 430 Ma but weakened to the south.

Implications for Subduction Polarity Reversal

The northern Proto-Tethys Ocean is considered to have subducted southward since ca. 530 Ma (Fig. 4A1), based on the ca. 525–494 Ma Kudi SSZ-type ophiolite (Li and Zhang, 2014), forearc basin, and arc magmatism in the south (Xiao et al., 2002). Subsequently, the Cambrian SSZ-type ophiolites, volcanic and sedimentary rocks collided with the SW Tarim Craton (Fig. 4A2), resulting in formation of a series of NW-vergent imbricated thrusts along the northern margin of the southern Kunlun terrane (Fig. 1C; Xiao et al., 2003). At ca. 487–485 Ma, a new subduction zone developed in the southern Proto-Tethys Ocean, as indicated by the magmatic sequence of forearc basalt-like gabbros, boninites (ca. 487 Ma) and Nb-enriched gabbros (ca. 485 Ma) in the Qimanyute Ophiolite (Zhang et al., 2021). Evidence for northward subduction of the southern Proto-Tethys Ocean is clear in the southern margin of the southern Kunlun terrane, where the Ordovician subduction complex is characterized by a series of SE-vergent thrusts (Fig. 1C; Xiao et al., 2003). In addition, the temporal, spatial, and petrogenetic relations of ca. 485–430 Ma arc magmatism in Tarim and southern Kunlun terrane imply that the southern Proto-Tethys Ocean subducted northward beneath the southern Kunlun terrane and Tarim (Fig. 4A3). We therefore propose that a reversal in subduction polarity is marked by an abrupt change (~2 Myr) of arc magmas from the island arc series with radiogenetic Hf-Nd isotopes to the calc-alkaline series with nonradiogenetic Hf-Nd isotopes at ca. 487–485 Ma. Combined with the short time interval between the minimum age (494 ± 1 Ma) of the Kudi ophiolite and the maximum age (487 ± 2 Ma) of Qimanyute ophiolite, we argue that subduction polarity reversal occurred in a transient period (7 ± 3 Ma), similar to other orogens (e.g., Taiwan; Clift et al., 2003; Fuping arc; Ning et al., 2020).

In the classic polarity reversal model, buoyancy contrast between continental and oceanic crust after arc-continent collision will lead to slab break-off or tearing followed by

exhumation of continental-type (U)HP rocks and high-flux magmatism, such as the Taiwan and Alps orogens (Clift et al., 2003; Malusà et al., 2011). Numerical modeling suggests a ca.10–25 Ma interval between initial collision and subsequent slab break-off for a normal oceanic slab (van Hunen and Allen, 2011). Therefore, rapid polarity reversal (within 10 Ma) indicates that slab break-off is not the responsible mechanism in the WKOB. Furthermore, the lack of voluminous magmatism (ca. 480 Ma; Fig. 1D) and no exhumation of (U)HP rocks in the WKOB after the collision is inconsistent with rapid polarity reversal caused by slab tearing (e.g., Taiwan; Clift et al., 2003).

Recent numerical modelling suggests that polarity reversal is more likely to occur under the ideal combination of thermo-mechanical conditions, of an older DP and relatively younger OP. This will specifically favor OP-DP coupling prior to slab break-off (Almeida et al., 2022). To test this hypothesis, we conducted two-dimensional numerical modeling in which the DP (northern Proto-Tethys Ocean) was older than the OP (southern Proto-Tethys Ocean) (Table DR6–7; see details in the Supplemental Material), as inferred from the ages of ophiolites in the WKOB (Li and Zhang, 2014; Zha et al., 2022).

Our modeling shows how subduction polarity reversal initiates and evolves (Fig. 4B), and is supported by geological observations in the WKOB. During the Cambrian, the northern Proto-Tethys Ocean was subducted southwards to form an intra-oceanic arc represented by the southern Kunlun terrane (Fig. 4B1). At ca. 490 Ma, the collision between the Tarim Craton and southern Kunlun terrane closed the northern Proto-Tethys Ocean. Subsequently, subduction of the northern Proto-Tethys oceanic plate was interrupted by the sinking southern Proto-Tethys Ocean plate, and these two plates rapidly became coupled at depth (Fig. 4B2). This plate coupling resulted in the northern Proto-Tethys oceanic plate pulling the southern Proto-Tethys oceanic plate downwards by accelerating the northward subduction of southern Proto-Tethys ocean and blocking the upwelling of the asthenosphere (Fig. 4B2). Subsequent subduction of the southern Proto-Tethys oceanic plate carried the subducting continental crust into the mantle, preventing the rebound of the positively buoyant relic rocks (Fig. 4B3). The coupling between the OP and DP implies that polarity reversal may happen more quickly than

previously thought, because time for the deepest part of the slab to break-off and sink far enough to make space for a new slab is no longer rate limiting. The influence of plate coupling in subduction polarity reversal will fundamentally change the course of orogenesis and its tectonomagmatic expression, and hence it provides a new example of polarity reversal-modified arc-continent collision orogeny, which may be applicable in other orogenic belts.

ACKNOWLEDGEMENTS

This study was financially supported by the National Key Research and Development Project (No. 2022YFC2903302) and Natural Science Foundation of China (No. 41888101). This is a contribution to IGCP 662.

Figure captions

Figure 1. (A) Simplified tectonic map of the major cratons and orogenic belts in China. (B) Simplified geologic map of the WKOB (modified after Zhang et al., 2018), (C) Cross-section across the A–B line (modified after Xiao et al., 2003) and (D) zircon U-Pb geochronological framework of Paleozoic magmatism in the WKOB.

Figure 2. Plots showing (A–B) whole-rock $\varepsilon_{Nd}(t)$ and zircon $\varepsilon_{Hf}(t)$ versus age; (C) Th/Yb versus Nb/Yb ratios (Pearce, 2008); (D) whole-rock $^{143}Nd/^{144}Nd(t)$ versus Sm/Nd ratios; (E–F) the variations of Th/Sm ratios with time and space for 530–430 Ma magmatic rocks (SiO_2 = 43–56 wt.%) in the WKOB. Data sources: Depleted mantle (Zhang et al., 2021). GLOSS (Plank and Langmuir 1998); CABs and IABs (Kelemen et al., 2003); ca. 0.8 Ga mafic rocks (SW Tarim Craton; Zhang et al., 2010); ca. 2.4 Ga basalts rocks (Tianshuihai terrane; Ji et al., 2011).

Figure 3. Histograms and normalized probability curves for the detrital zircon ages of the early Paleozoic sedimentary samples in the WKOB.

Figure 4. Cartoon (A1–A3) and numerical modelling (B1–B3) illustrate geodynamic model for the subduction polarity reversal in the WKOB during early Paleozoic. Key physical parameters of the numerical model are provided in Table DR6-7.

REFERENCES CITED

Almeida, J., Riel, N., Rosas, F.M., Duarte, J.C., and Schellart, W.P., 2022, Polarity-reversal subduction zone initiation triggered by buoyant plateau obstruction: Earth and Planetary Science Letters, v. 577, p. 117195, https://doi .org/10.1016/j.epsl.2021.117195.

Crameri, F., Magni, V., Domeier, M., Shephard, G.E., Chotalia, K., Cooper, G., Eakin, C.M., Grima, A.G., Gürer, D., Király, Á., Mulyukova, E., Peters, K., Robert, B., and Thielmann, M., 2020, A transdisciplinary and community-driven database to unravel subduction zone initiation: Nature Communications, v. 11, p. 1–14, https://doi .org /10 .1038 /s41467 -020 -17522 -9.

Clift, P.D., Schouten, H., and Draut, A.E., 2003, A general model of arc-continent collision and subduction polarity reversal from Taiwan and the Irish Caledonides, in Larter, R.D. and Leat, P.T., eds., Intra-Oceanic Subduction Systems: Tectonic and Magmatic Processes: Geological Society of London, Special Publication, v. 219, p. 81–98, https://doi .org/10.1144/GSL.SP.2003.219.01.04.

Ji, W.H., Li, R.S., Chen, S.J., He, S.P., Zhao, Z.M., Bian, X.W., Zhu, H.P., Cui, J.G., and Ren, J.G., 2011, The discovery of Paleoproterozoic volcanic rocks in the Bulunkuole Group from the Tianshuihai massif in Xinjiang of northwest China and its geological

262 significance: Science China Earth Sciences, v. 54, p. 61-72,
263 https://doi.org/10.1007/s11430-010-4043-7.

264 Kelemen, P.B., Hanghøj, K., and Greene, A., 2003, One view of the geochemistry of
265 subduction-related magmatic arcs, with an emphasis on primitive andesite and lower
266 crust, in Holland, H.D., and Turekian, K.K., eds., Treatise on geochemistry, Volume 3:
267 Oxford, Elsevier, p. 593-659.

268 Kerr, A.C., White, R.V., Thompson, P.M.E., Tarney, J., and Saunders, A.D. 2003, No oceanic
269 plateau - No Caribbean Plate? The seminal role of an oceanic plateau in Caribbean plate
270 evolution. In: Bartolini, C., Buffler, R.T. & Blickwede, J. (eds) The Circum Gulf of
271 Mexico and Caribbean: Hydrocarbon Habitats Basin Formation and Plate Tectonics:
272 American Association of Petroleum Geology Memoir, v. 79, p. 126-268,
273 http://dx.doi.org/10.1306/M79877C6.

274 Kusky, T. M., and Kidd, W.S.F., 1996, Tectonic Implications of Early Silurian Thrust
275 Imbrication of the Northern Exploits Subzone, central Newfoundland: Journal of
276 Geodynamics, v. 22, p. 229-265, http://dx.doi.org/10.1016/0264-3707(96)00011-7.

277 Kusky, T.M., Polat, A., Windley, B.F., Burke, K.C., Dewey, J.F., Kidd, W.S.F., Maruyama,
278 S., Wang, J.P., Deng, H., Wang, Z.S. Wang, C., Fu, D., Li, X.W., and Peng, H.T., 2016,
279 Insights into the tectonic evolution of the North China Craton through comparative
280 tectonic analysis: A record of outward growth of Precambrian continents: Earth Science
281 Reviews, v. 162, p. 387-432, http://dx.doi.org/10.1016/j.earscirev.2016.09.002.

282 Li, T.F., and Zhang, J.X., 2014, Zircon LA-ICP-MS U-Pb ages of websterite and basalt in
283 Kudi ophiolite and the implication, West Kunlun: Acta Petrologica Sinica, v. 30, p.
284 2393–2401 (in Chinese with English abstract).

285 Liu, X.Q., Zhang, C.L., Ye, X.T., Zou, H.B., and Hao, X.S., 2019, Cambrian mafic and
286 granitic intrusions in the Mazar-Tianshuihai terrane, West Kunlun Orogenic Belt:

Constraints on the subduction orientation of the Proto-Tethys Ocean: Lithos, v. 350–351, p. 105226, https://doi.org/10.1016/j.lithos.2019.105226.

Mann, P., and Taira, A., 2004, Global tectonic significance of the Solomon Islands and Ontong Java Plateau convergent zone: Tectonophysics, v. 389, p. 137–190, https://doi.org/10.1016/j.tecto.2003.10.024.

Malusà, M. G., Faccenna, C., Garzanti, E., and Polino, R., 2011, Divergence in subduction zones and exhumation of high pressure rocks (Eocene Western Alps): Earth and Planetary Science Letters, v. 310, p. 21–32, https://doi.org/10.1016/j.epsl.2011.08.002.

Ning, W.B., Kusky, T, Wang, J.P., Wang, L., Deng, H., Polat, A., Huang, B., Peng, H.T., and Feng, P., 2020, From subduction initiation to arc-polarity reversal: Life cycle of an Archean subduction zone from the Zunhua ophiolitic mélange, North China Craton: Precambrian Research, v. 350, 105868, https://doi.org/10.1016/j.precamres.2020.105868.

Pearce, J.A., 2008, Geochemical fingerprinting of oceanic basalts with applications to ophiolite classification and the search for Archean oceanic crust: Lithos, v. 100, p. 14-48, https://doi.org/10.1016/j.lithos.2007.06.016.

Plank, T., and Langmuir, C.H., 1998, The chemical composition of subducting sediment and its consequences for the crust and mantle: Chemical Geology, v. 145, p. 325–394, https://doi.org/10.1016/S0009-2541(97)00150-2.

Stern, R.J., Reagan, M., Ishizuka, O., Ohara, Y., and Whattam, S., 2012, To understand subduction initiation, study forearc crust: To understand forearc crust, study ophiolites: Lithosphere, v. 4, p. 469–483, https://doi.org/10.1130/L183.1.

Stern, R.J., and Gerya, T., 2018, Subduction initiation in nature and models: a review: Tectonophysics, v. 746, p. 173-198, https://doi.org/10.1016/j.tecto.2017.10.014.

Teng, L.S., Lee, C.T., Tsai, Y.B., and Hsiao, L.Y., 2000, Slab breakoff as a mechanism for flipping of subduction polarity in Taiwan: Geology, v. 28, p. 155–158, https://doi.org/10.1130/0091-613(2000)28<155:SBAAMF>2.0.CO;2.

van Hunen, J., and Allen, M.B., 2011, Continental collision and slab break-off: A comparison of 3-D numerical models with observations: Earth and Planetary Science Letters, v. 302, p. 27–37, https://doi .org/10.1016/ j.epsl.2010.11.035.

Wang, P., Zhao, G.C., Liu, Q., Yao, J.L., Han, Y.G., and Li, J.H., 2022, Effect of source compositions on adakitic features: A case study from the Buya granite, in western Kunlun, NW China: American Journal of Science, v. 322, p. 828-850, https://doi.org/10.2475/06.2022.03.

Xiao, W.J., Windley, B.F., Hao, J., and Li, J.L., 2002, Arcophiolite obduction in the Western Kunlun Range (China): Implications for the Palaeozoic evolution of central Asia: Journal of the Geological Society, v. 159, p. 517–528, https://doi .org/10.1144/0016-764901-093.

Xiao, W.J., Han, F.L., Windley, B.F., Yuan, C., Zhou, H., and Li, J.L., 2003, Multiple accretionary orogenesis and episodic growth of continents: Insights from the western Kunlun Range, Central Asia: International Geology Review, v. 45, p. 303–328, https://doi .org/10.2747/0020-6814.45.4.303.

Zha, XF., Dong, YP., Gao, XF., Ji, WH., Liu, XM., He, DF., Li, P., Zhang, HD., and Yang, C., 2022, The Early Paleozoic Subashi ophiolite in the West Kunlun Orogenic Belt (northwestern Tibetan Plateau): Implication for the tectonic evolution of the Proto-Tethys: Journal of Asian Earth Sciences, v. 238, p. 105388, https://doi .org/10.1016/j.jseaes.2022.105388.

Zhang, C.L., Yang, D.S., Wang, H.Y., Dong, Y.G., and Ye, H.M., 2010, Neoproterozoic Mafic Dykes and Basalts in the Southern Margin of Tarim, Northwest China: Age, Geochemistry and Geodynamic Implications: Acta Geologica Sinica (English Edition), v. 84, p. 549–562, https://doi.org/10.1111/j.1755-6724.2010.00200.x.

337 Zhang, C.L., Zou, H.B., Ye, X.T., Chen, X.Y., 2018, Timing of subduction initiation in the
338 Proto-Tethys Ocean: Evidence from the Cambrian gabbros from the NE Pamir Plateau:
339 Lithos, v. 314-315, p. 40-51, https://doi.org/10.1016/j.lithos.2018.05.021.

340 Zhang, C.L., Zou, H.B., Ye, X.T., and Chen, X.Y., 2019, Tectonic evolution of the West
341 Kunlun Orogenic Belt along the northern margin of the Tibetan Plateau: Implications for
342 the assembly of the Tarim terrane to Gondwana: Geoscience Frontiers, v. 10, p. 973–988,
343 https://doi.org/10.1016/ j.gsf.2018.05.006.

344 Zhang, Q.C., Li, Z.H., Wu, Z.H., Chen, X.H., Zhang, J.E., and Yang, Y., 2021, Subduction
345 initiation of the western Proto-Tethys Ocean: New evidence from the Cambrian intra-
346 oceanic forearc ophiolitic mélange in the western Kunlun Orogen, NW Tibetan Plateau:
347 Geological Society of America bulletin, v. 134, p. 145-159,
348 https://doi.org/10.1130/B35922.1.

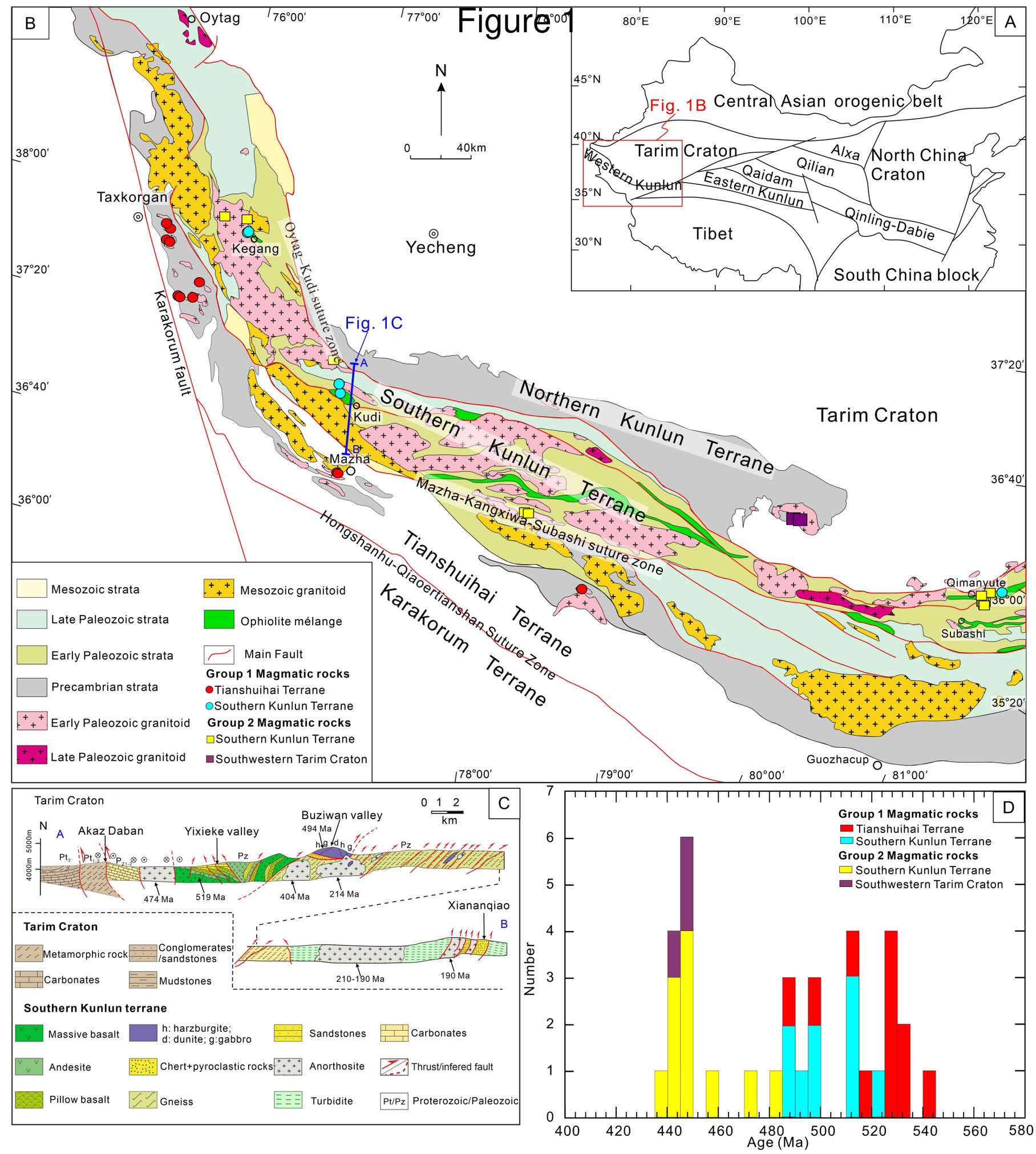
Figure1
B
A
C
D
Oytag
Taxkorgan
Kegang
Yecheng
Kudi
Mazha
Qimanyute
Subashi
Guozhacup
Karakorum fault
Oytag–Kudi suture zone
Fig. 1C
Northern Kunlun Terrane
Southern Kunlun Terrane
Tarim Craton
Mazha-Kangxiwa-Subashi suture zone
Hongshanhu-Qiaoertianshan Suture Zone
Tianshuihai Terrane
Karakorum Terrane
N
0 40km
76°00′
77°00′
78°00′
79°00′
80°00′
81°00′
38°00′
37°20′
36°40′
36°00′
35°20′
80°E
90°E
100°E
110°E
120°E
45°N
40°N
35°N
30°N
Fig. 1B
Central Asian orogenic belt
Tarim Craton
Western Kunlun
Alxa
North China Craton
Qilian
Qaidam
Eastern Kunlun
Qinling-Dabie
Tibet
South China block
Mesozoic strata
Late Paleozoic strata
Early Paleozoic strata
Precambrian strata
Early Paleozoic granitoid
Late Paleozoic granitoid
Mesozoic granitoid
Ophiolite mélange
Main Fault
Group 1 Magmatic rocks
Tianshuihai Terrane
Southern Kunlun Terrane
Group 2 Magmatic rocks
Southern Kunlun Terrane
Southwestern Tarim Craton
Tarim Craton
N
A
Akaz Daban
Yixieke valley
Buziwan valley
494 Ma
Pz
Pt3
Pt1,2
Pz1,2
4000m
5000m
474 Ma
519 Ma
404 Ma
214 Ma
0 1 2
km
Xiananqiao
B
210-190 Ma
190 Ma
Tarim Craton
Metamorphic rock
Conglomerates /sandstones
Carbonates
Mudstones
Southern Kunlun terrane
Massive basalt
h: harzburgite;
d: dunite; g:gabbro
Sandstones
Carbonates
Andesite
Chert+pyroclastic rocks
Anorthosite
Thrust/infered fault
Pillow basalt
Gneiss
Turbidite
Pt/Pz
Proterozoic/Paleozoic
Group 1 Magmatic rocks
Tianshuihai Terrane
Southern Kunlun Terrane
Group 2 Magmatic rocks
Southern Kunlun Terrane
Southwestern Tarim Craton
Number
Age (Ma)
0
1
2
3
4
5
6
7
400
420
440
460
480
500
520
540
560
580

Figure 2

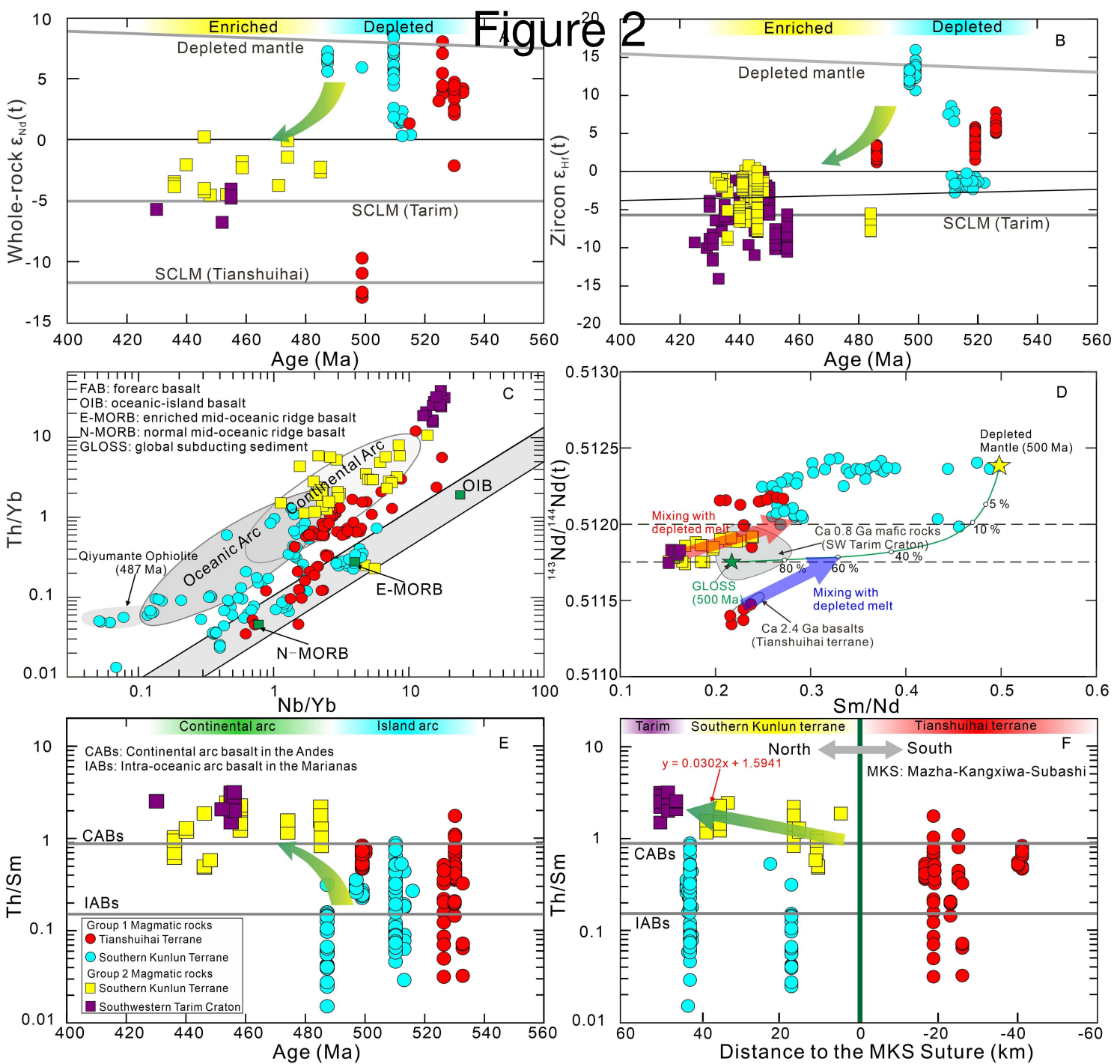
A
Enriched
Depleted
Depleted mantle
SCLM (Tarim)
SCLM (Tianshuihai)
Whole-rock $\varepsilon_{Nd}(t)$
Age (Ma)
B
Zircon $\varepsilon_{Hf}(t)$
C
FAB: forearc basalt
OIB: oceanic-island basalt
E-MORB: enriched mid-oceanic ridge basalt
N-MORB: normal mid-oceanic ridge basalt
GLOSS: global subducting sediment
Continental Arc
Oceanic Arc
OIB
E-MORB
N-MORB
Qiyumante Ophiolite (487 Ma)
Th/Yb
Nb/Yb
D
Depleted Mantle (500 Ma)
5 %
10 %
40 %
60 %
80 %
Mixing with depleted melt
Ca 0.8 Ga mafic rocks (SW Tarim Craton)
GLOSS (500 Ma)
Mixing with depleted melt
Ca 2.4 Ga basalts (Tianshuihai terrane)
$^{143}Nd/^{144}Nd(t)$
Sm/Nd
E
Continental arc
Island arc
CABs: Continental arc basalt in the Andes
IABs: Intra-oceanic arc basalt in the Marianas
CABs
IABs
Group 1 Magmatic rocks
Tianshuihai Terrane
Southern Kunlun Terrane
Group 2 Magmatic rocks
Southern Kunlun Terrane
Southwestern Tarim Craton
Th/Sm
Age (Ma)
F
Tarim
Southern Kunlun terrane
Tianshuihai terrane
North
South
y = 0.0302x + 1.5941
MKS: Mazha-Kangxiwa-Subashi
CABs
IABs
Th/Sm
Distance to the MKS Suture (km)

Figure 3

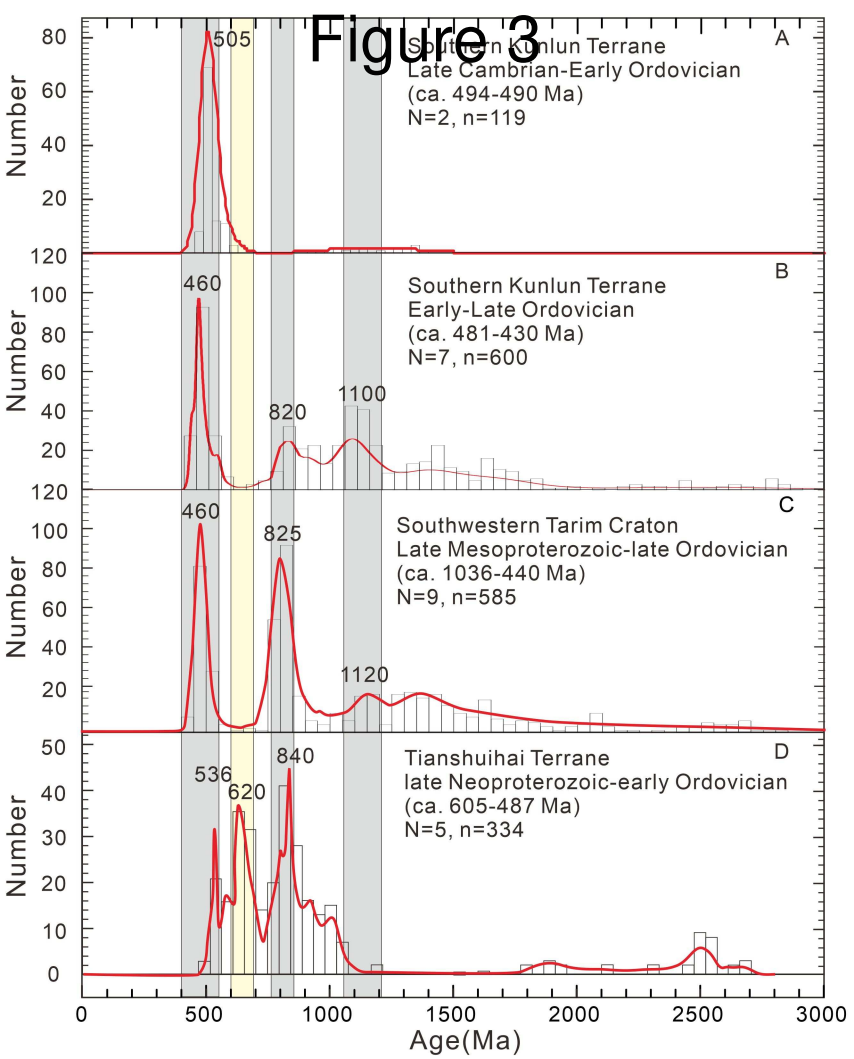
A
Southern Kunlun Terrane
Late Cambrian-Early Ordovician
(ca. 494-490 Ma)
N=2, n=119
505
B
Southern Kunlun Terrane
Early-Late Ordovician
(ca. 481-430 Ma)
N=7, n=600
460
820
1100
C
Southwestern Tarim Craton
Late Mesoproterozoic-late Ordovician
(ca. 1036-440 Ma)
N=9, n=585
460
825
1120
D
Tianshuihai Terrane
late Neoproterozoic-early Ordovician
(ca. 605-487 Ma)
N=5, n=334
536
620
840
Number
Age(Ma)
0
500
1000
1500
2000
2500
3000

Figure 4

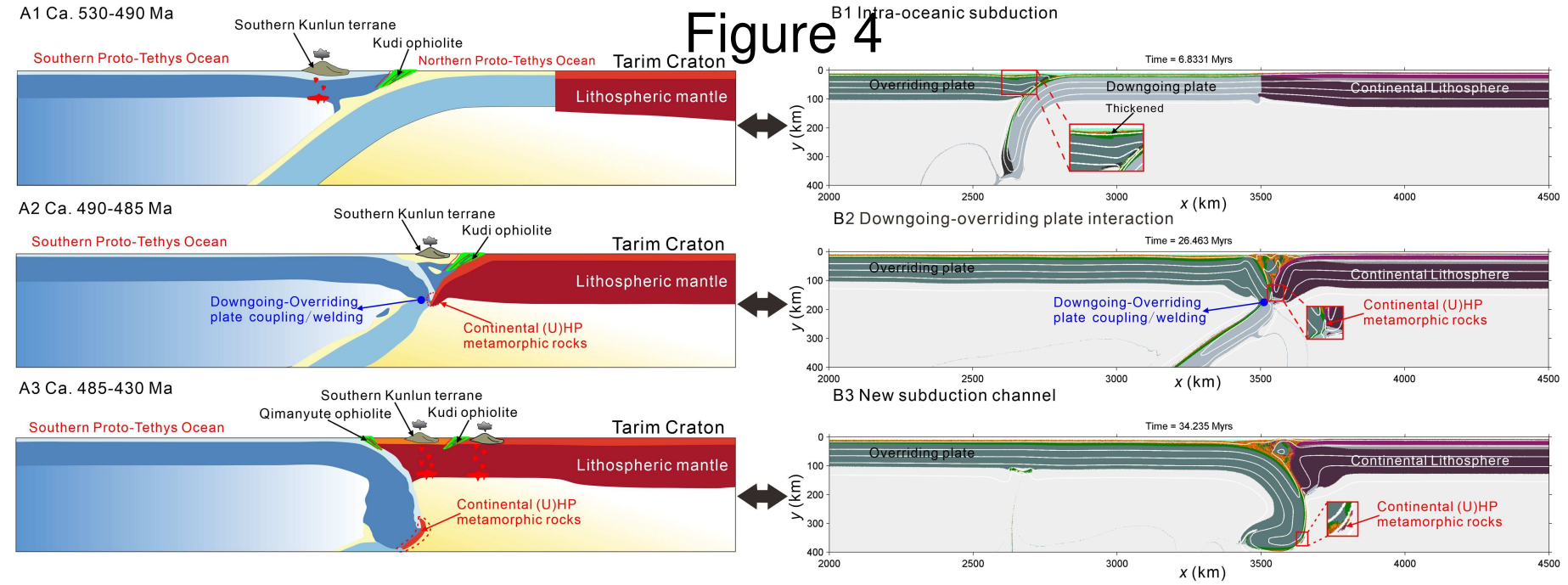
A1 Ca. 530-490 Ma
Southern Kunlun terrane
Kudi ophiolite
Southern Proto-Tethys Ocean
Northern Proto-Tethys Ocean
Tarim Craton
Lithospheric mantle
B1 Intra-oceanic subduction
Time = 6.8331 Myrs
Overriding plate
Downgoing plate
Thickened
Continental Lithosphere
y (km)
x (km)
A2 Ca. 490-485 Ma
Southern Kunlun terrane
Kudi ophiolite
Southern Proto-Tethys Ocean
Tarim Craton
Lithospheric mantle
Downgoing-Overriding
plate coupling/welding
Continental (U)HP
metamorphic rocks
B2 Downgoing-overriding plate interaction
Time = 26.463 Myrs
Overriding plate
Continental Lithosphere
Downgoing-Overriding
plate coupling/welding
Continental (U)HP
metamorphic rocks
y (km)
x (km)
A3 Ca. 485-430 Ma
Southern Kunlun terrane
Qimanyute ophiolite
Kudi ophiolite
Southern Proto-Tethys Ocean
Tarim Craton
Lithospheric mantle
Continental (U)HP
metamorphic rocks
B3 New subduction channel
Time = 34.235 Myrs
Overriding plate
Continental Lithosphere
Continental (U)HP
metamorphic rocks
y (km)
x (km)